Electronic Supplementary Information (ESI)

Designing a new family of oxonium-cation based structurally diverse organic-inorganic hybrid iodoantimonate crystals

Swati Parmar, [a] Shiv Pal, [a] Abhijit Biswas,[a] Suresh Gosavi, [b,c] Sudip Chakraborty, *[d] Mallu Chenna Reddy*[a] and Satishchandra Ogale*[a]

[a]Department of Physics and Centre for Energy Science, IISER Pune, Maharashtra-411008, India

[b]Department of Technology, Savitribai Phule Pune University, Maharashtra-411007, India

[c]Department of Physics, Savitribai Phule Pune University, Maharashtra-411007, India

[d]Discipline of Physics, Indian Institute of Technology, Indore - 453552, Madhya Pradesh, India

The Supporting information contains instrumental details, FESEM images, PXRD spectra, Raman Spectra, FTIR Spectra, DSC and TGA Spectra, single crystal XRD details and computational details. The Crystallographic information file (CIF) has been submitted to Cambridge Crystallographic Data Centre (CCDC) and CCDC numbers are 1910951, 1910947, 1910950 and 1910948 for 1, 2, 3 and 4 respectively.

*Corresponding authors. E-mail: satishogale@iiserpune.ac.in, mchenna@students.iiserpune.ac.in, sudiphys@gmail.com

Table of Contents

Contents	Page Number
Characterisation	S3
Materials	S3
Thin Film Fabrication	S3-S4
Single Crystal XRD Description	S4
Figure S1	S5
Figure S2	S6
Figure S3	S7
Table 1	S7
Figure S4	S7
Figure S5	S8
Figure S6	S9
Figure S7	S10
Table 2	S11-S12
Table 3	S13-S14
Computational Methodology	S14-S15
Figure S8	S15
Figure S9	S16
References	S16

I. Instrumental Details

Characterization Technique:

Field emission scanning electron microscopy (FESEM, JEM-2100F, JEOL, Japan) and Energy-dispersive X-rays (EDAX) was used to perform the morphology and elemental analysis of as-prepared crystals. The powder X-ray diffraction (PXRD) (Bruker D8-Advance X-ray diffractometer (Germany) with Cu Kα radiation (λ = 1.5418 Å)) was used to record the experimental PXRD pattern. To record the absorption spectra of as-prepared crystals, ultraviolet-visible (UV–vis) spectrophotometer (LAMBDA 950, PerkinElmer) was used. A Horiba Scientific FluoroMax-4 spectrofluorometer was used to record the PL spectra at various wavelengths. Time-resolved PL measurements were performed using FLS 980 (Edinburgh Instruments) at the emission peaks of the respective perovskite films. We used UV light (365 nm) for recording images in the dark. Raman spectra of crystals were recorded with RENISHAW spectrometer using a diode laser (wavelength 532 nm) in the backscattering geometry. FTIR spectra were recorded using a Nicolet ID5 attenuated total reflectance IR spectrometer which operates at ambient temperature. Thermal analysis (thermo-gravimetric) were carried out using NETSZCH TGA-DSC system. TGAs were performed under 20 ml/min N_2 gas flow (purge + protective) and the heating rate was maintained 5 K/min from 25°C to 550°C.

II. Materials:

The commercially available chemicals, Antimony(III) oxide (Sb_2O_3, 99.99%) was purchased from Sigma Aldrich, Hydriodic acid (HI) ≥57 wt. % in H_2O was purchased from Merck, N,N-dimethylformamide (DMF) (anhydrous, 99.8%), 2-pyrrolidinone (2-Pyrr.) (anhydrous, 99.8%), N-methyl-2-pyrrolidone (NMP) (anhydrous, 99.8%) and dimethylacetamide (DMA) (anhydrous, 99.8%) were purchased from Sigma-Aldrich. The aforementioned chemicals were used as-purchased without any purification.

$(DMF\text{-}H\bullet\bullet\bullet DMF)_2Sb_2I_9$ (**1**), $(2\text{-pyrr.-}H\cdots 2\text{-pyrr.})_2Sb_2I_8$ (**2**), $(NMP\text{-}H\bullet\bullet\bullet NMP)_3Sb_3I_{12}$ (**3**) and $(DMA\text{-}H\bullet\bullet\bullet DMA)_2Sb_2I_9$ (**4**) were prepared by adding 37 mg Sb_2O_3 in 2 mL hydroiodic acid, followed by continuous stirring and heating at 100 °C till it dissolves completely. Then, 2 mL of respective solvent was added drop wise into the Sb_2O_3 HI which resulted into turbid orange solution and subsequently, it was left at the same condition for 15 minutes, which led to a clear orange solution. The mixture was kept undisturbed for good quality crystal growth. After half an hour, nice orange colour crystals were formed in case of **1** and **4**. When this mixture was kept further for 12 hours good quality large size crystals were grown, whereas **2** and **3** requires 6-7 days for complete growth of the crystals due to different nucleation rate of cyclic solvents. The crystals were then collected after filtering and washing with ethyl acetate to remove the surface impurities.

III. Thin Film Fabrication

The thin film fabrication was done in order to perform the charge transfer between Au, **1** and **2**. The Au thin film of 10 nm was deposited by using pulsed laser deposition (λ=248 nm, KrF excimer laser) technique on quartz substrate at room temperature, 1000 laser shots at 5 Hz frequency. Then **1** and **2** were deposited by spin coating method. The solution for spin coating was prepared by dissolving the respective crystals in their respective solvent (60 mg crystal in 200 µl solvent) and spin coated the solution on Au/quartz film at 1500 rpm for 60 seconds.

IV. Single Crystal XRD

Crystal was coated with Paratone-N oil, attached to a Kapton loop and transferred to a Bruker D8 Venture Diffractometer equipped with a Photon 100CMOS detector. Frames were collected using ϕ and ω scans and the unit-cell parameters were refined against all data. The

crystals did not show significant decay during data collection. Data was integrated and corrected for Lorentz and polarization effects using SAINT 8.27b, and were collected for absorption effects using SADABS V2012. The structures were solved by direct methods and expanded through successive difference Fourier maps using SHELXTL-2013 software package. Hydrogen atoms were inserted at idealized positions and refined using a riding model with an isotropic thermal parameter 1.2 times that of the attached carbon atom or 1.5 times that of the attached nitrogen. Details regarding the data quality and a summary of residual values of the refinement are listed in Table S2 and S3. The simulated XRD pattern is found to match well with the PXRD data collected, see Figure S2 and S3. crystal X-ray diffraction.

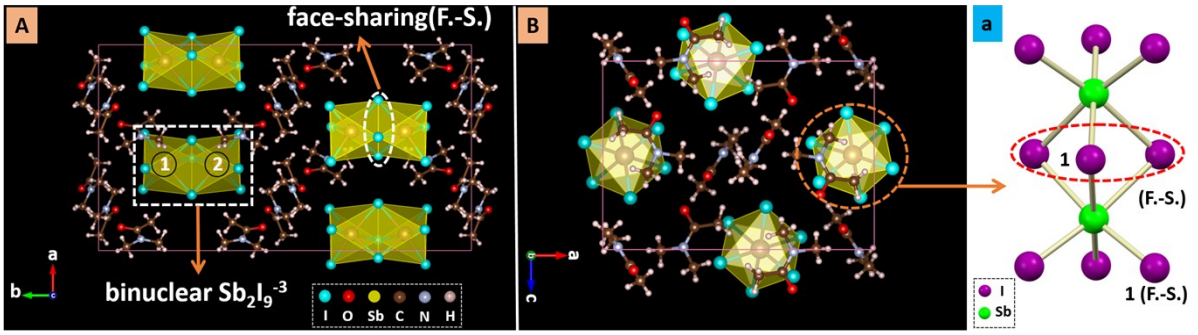

Figure S1 Left column: X-ray crystal structures of compounds **4** (top view) showing bi-nuclear anion $(Sb_2I_9)^{3-}$ (A); Middle column: X-ray crystal structures of compounds **4** from the side view (B); Right column: a clear representation of the number of face and edge-sharing units of compounds **4** in ball and stick model (SXRD) (a).

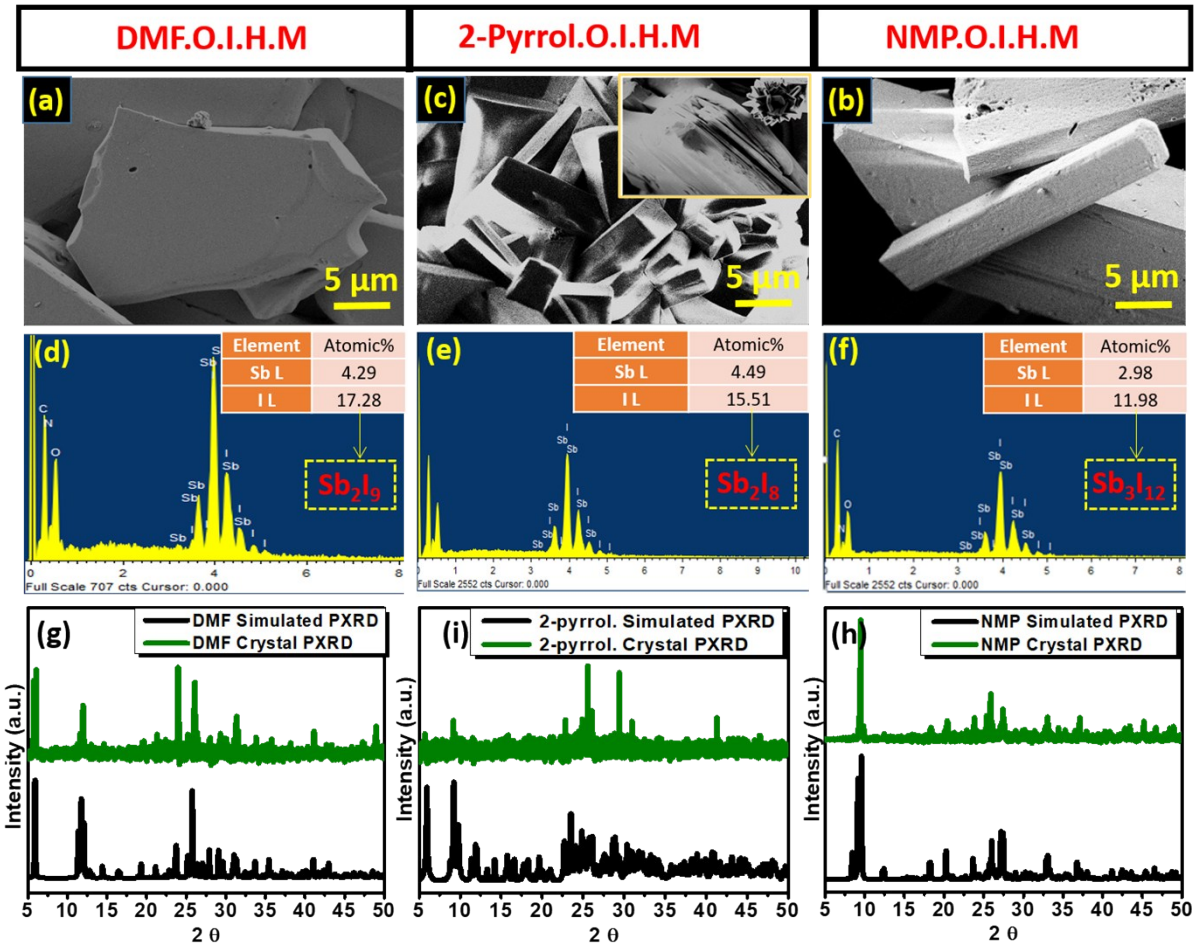

Figure S2 Morphological and Structural Characterization. (a-c) Top view of FESEM image of as-synthesised crystals morphology of the **1, 2** and **3.** **(c)** Inset depicts the fine quality of the crystal cross-section. **(d-f)** EDAX image of crystals depicting the Sb to I ratio in the crystal system. **(g-i)** shows the X-Ray Diffraction (XRD) spectra of **1, 2** and **3**, the black curve indicates the Simulated Powder XRD (PXRD) pattern obtained from single crystal and green curve indicate the experimental PXRD of **1,2** and **3.**

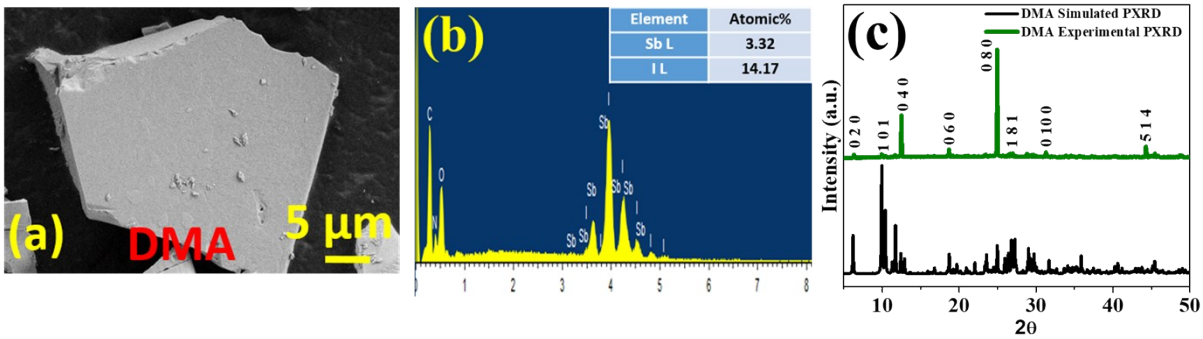

Figure S3 Morphological and Structural Characterization of **4**; (a) Top view of FESEM image of as-synthesised crystals morphology of **4**. (b) EDAX image of crystals depicting the Sb to I ratio in the crystal system of **4**; (c) shows the X-Ray Diffraction (XRD) spectra of **4**, black curve indicates the Simulated Powder XRD (PXRD) pattern obtained from single crystal and green curve indicate the experimental PXRD of **4**.

Table S1 EDAX atomic % of Sb and I element comprised in the single crystals of **1**, **2**, **3** and **4** respectively.

Crystals	Sb L (at. %)	I L (at. %)
DMF	4.29	17.28
2-Pyrrol.	4.49	15.51
NMP	2.98	11.98
DMA	3.32	14.17

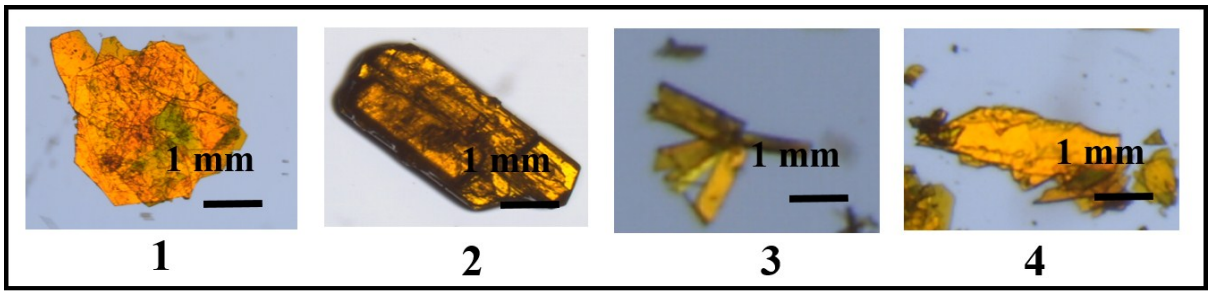

Figure S4 Optical microscopic images of **1**, **2**, **3** and **4** respectively.

V. Raman spectroscopy

In order to investigate the stretching and bending modes corresponding to the Sb-I inorganic moiety, Raman spectra are recorded in the frequency range of 100-300 cm^{-1}. These are shown in **Figure S5**. We basically observe three peaks at 105 cm^{-1}, 149 cm^{-1} and 162 cm^{-1}. Among these, first two correspond to the bending modes associated with the symmetric vibration of bridged iodide, and the symmetric and asymmetric vibrations of *trans* Sb-I. The 162 cm^{-1} one corresponds to the symmetric stretching mode of *cis* Sb-I. (Ref: 4)

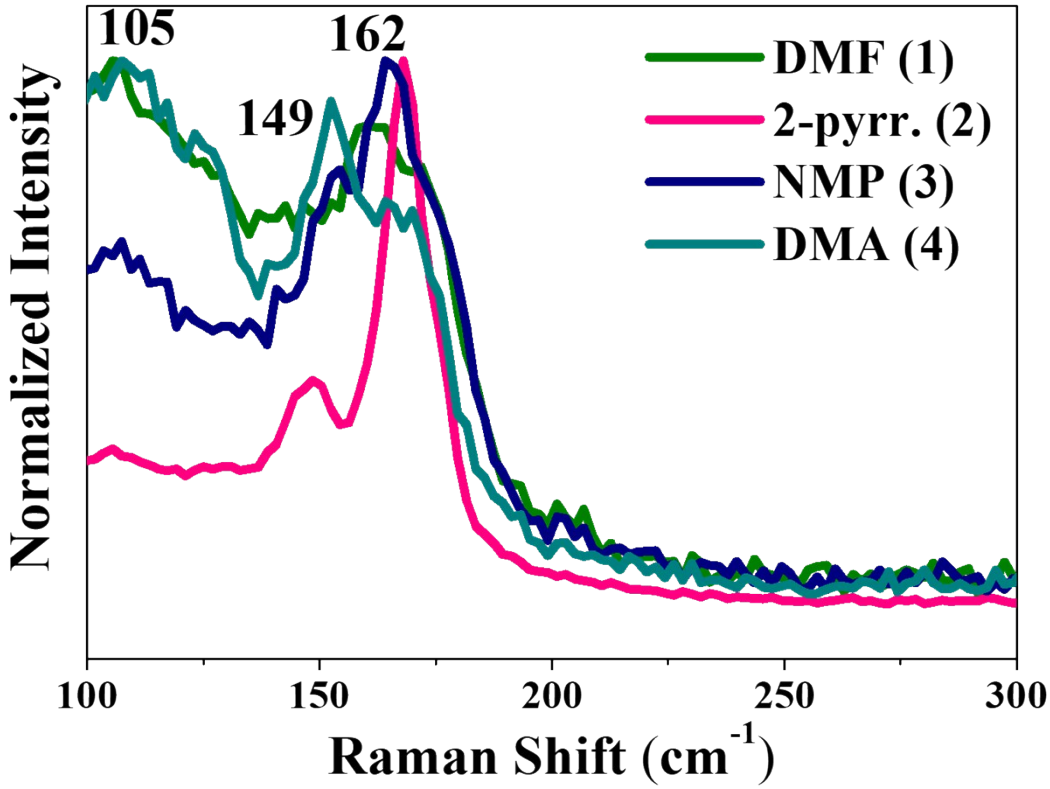

Figure S5 The Raman Spectra of **1**, **2**, **3** and **4**.

VI. Fourier-transform infrared spectroscopy (FTIR)

The vibrational IR spectra of **1** to **4** in the frequency range of 500 cm^{-1} to 4000 cm^{-1} are shown in **Fig. S6.** The important characteristic peaks of CO^{+}-H, C=O and C-H are the stretching frequencies of compounds **1-4**. The C(O)-H stretching frequency of formyl group from compound **1** and N-H stretching frequency of 2-pyrr. from compound **2** are also depicted.

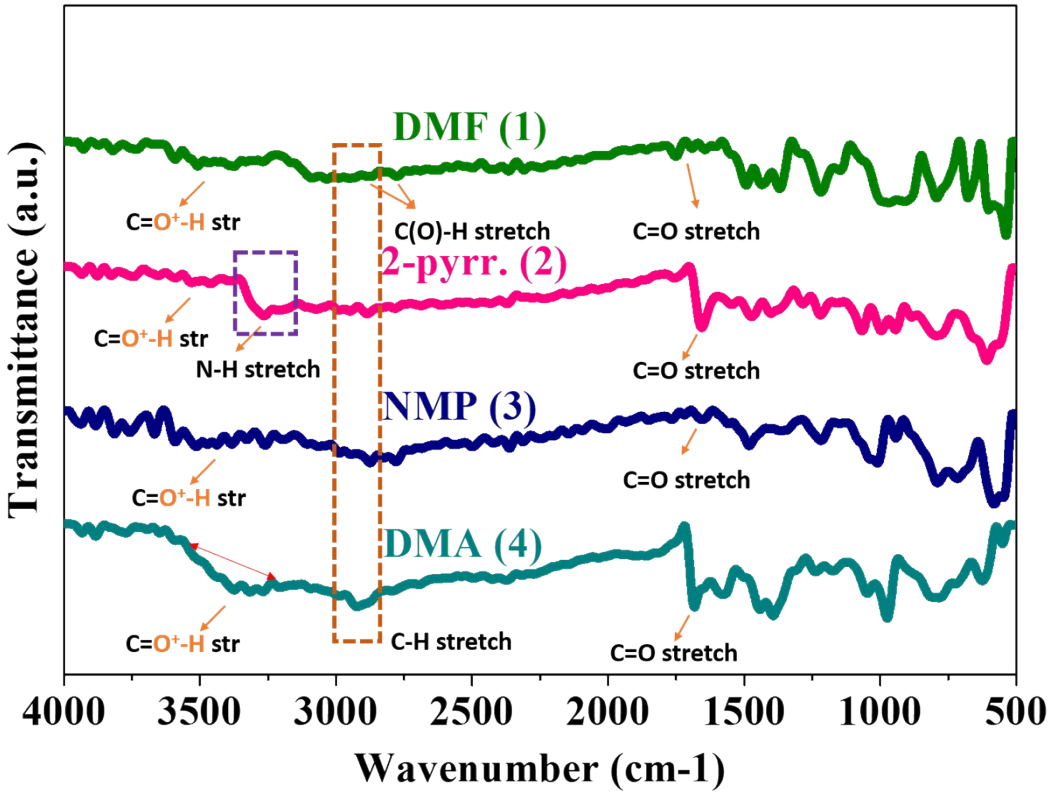

Figure S6 The Fourier-transform infrared spectroscopy (FTIR) data of **1** to **4** in the frequency range of 500 cm^{-1} to 4000 cm^{-1}**.**

VII. Thermal Analysis: Differential Scanning Calorimetry (DSC) and Thermogravimetric Analysis (TGA)

To examine the thermal properties of newly synthesised HOIMs **1** to **4,** TGA was performed from room temperature to 550 ºC under nitrogen flow. All the data are shown in **Fig S7.** The initial decomposition temperatures of **1** to **4** are about 180 ºC , 230 ºC, 220 ºC and 190 ºC, respectively, clearly indicating that the substituent on organic precursor of proton-bound oxonium salt plays an important role in the thermal stability of the corresponding HOIM. The compound **2** containing 2-pyrr. proton bounded oxonium cation shows more thermal stability as compared to others. The differential scanning calorimetry (DSC) data for the four cases are also shown in **Fig. S7** which conform to the TGA data.

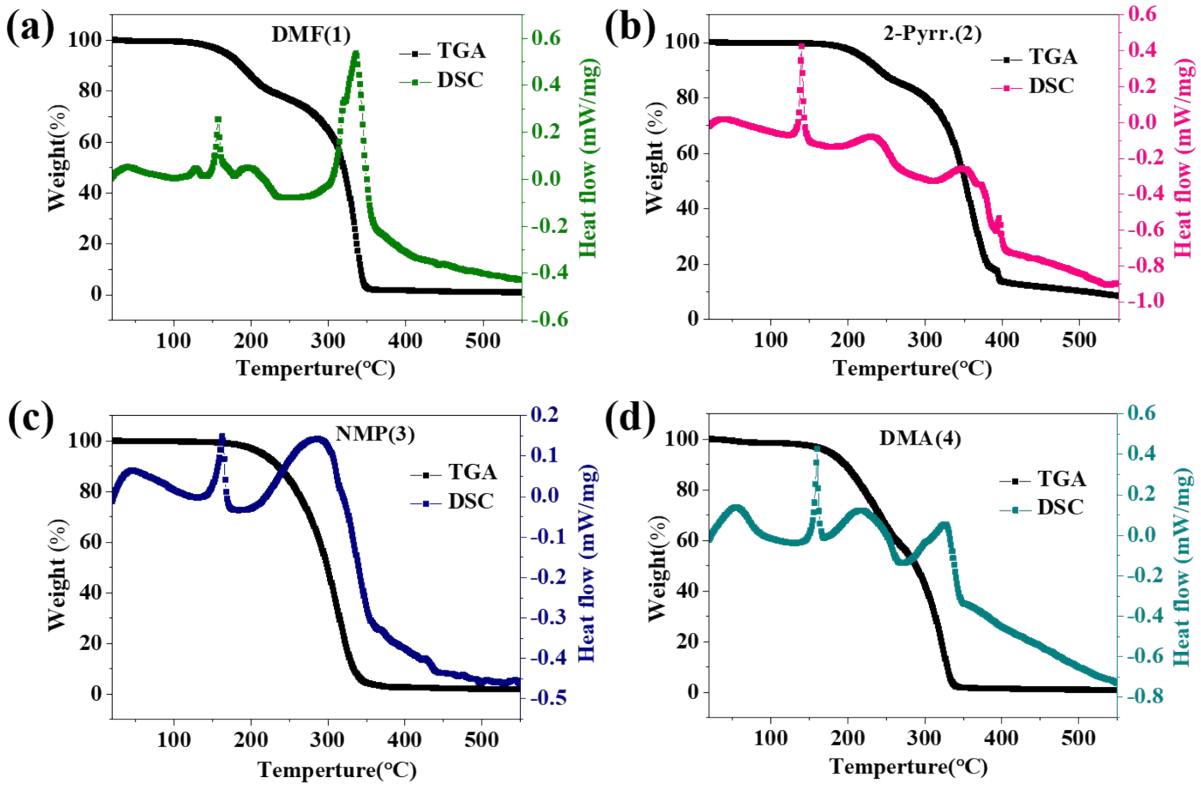

Figure S7 Differential Scanning Calorimetry and Thermogravimetric Analysis data for **1**, **2**, **3** and **4**, respectively.

VIII. Crystal data and structure refinement

Table S2 Crystal data and structure refinement for **DMF-Sb-I. O.I.H.M (1)**, **2-Pyrr.-Sb-I. O.I.H.M (2)** and **NMP-Sb-I. O.I.H.M (3).**

Compound name	***DMF-Sb-I.O.I.H.M***	***2-Pyrr.-Sb-I. O.I.H.M***	***NMP-Sb-I. O.I.H.M***
CCDC number	1910951	1910947	1910950
Empirical formula	$C_{12}\,H_{30}\,I_9\,N_4\,O_4\,Sb_2$ (+ squeezed protonated solvent)	$C_{16}\,H_{30}\,I_8\,N_4\,O_4\,Sb_2$	$C_{30}\,H_{57}\,I_{12}\,N_6\,O_6\,Sb_3$
Moiety formula representation	$Sb_2I_9(DMF\text{-}H\cdots DMF)_2$ (+ squeezed protonated solvent)	$Sb_2I_8(2\text{-}Pyrr.\text{-}H\cdots 2\text{-}Pyrr.)_2$	$Sb_3I_{12}(NMP\text{-}H\cdots NMP)_2$
Formula weight	1680.00	1601.14	2485.86
Temperature	150(2) K	150(2) K	150(2) K
Wavelength	0.71073 Å	0.71073 Å	0.71073 Å
Crystal system	orthorhombic	monoclinic	orthorhombic
Space group	'P n m a'	'P 21/n'	P n a 21
a	15.1734(8) Å	16.8665(6) Å	28.114(5) Å
b	30.0131(16) Å	10.9079(4) Å	11.329(2) Å
c	9.0791(4) Å	20.9932(7) Å	19.332(3) Å
α , β , γ	90°, 90°, 90°	90°, 107.1020(10)°, 90°	90°, 90 °, 90°
Volume	4134.6(4) $Å^3$	3691.5(2) $Å^3$	6157.3(18) $Å^3$
Z	4	4	4
Crystal size	108x135x11 mm	108x97x15 mm	200x110x32 mm
Density (calculated)	2.699 Mg/m^3	2.881 Mg/m^3	2.681 Mg/m^3
Absorption coefficient	8.047 mm^{-1}	8.180 mm^{-1}	7.361 mm^{-1}
F(000)	2964	2848	4452
Theta range for data collection	2.344 to 25.250°	2.254 to 25.250°	2.206 to 25.250°

Index ranges	-18<=h<=18 -35<=k<=36 -8<=l<=10	-20<=h<=20 -13<=k<=13 -25<=l<=25	-33 <=h<= 33 -13<=k<=13 -23<=l<= 23
Reflections collected	22566	75431	167392
Independent reflections	3819 [R(int) = 0.0537]	6671 [R(int) = 0.1027]	11146 [R(int) = 0.1635]
Completeness to theta = 25.242°	99.9 %	99.9 %	99.9 %
Refinement method	Full-matrix least-squares on F^2	Full-matrix least-squares on F^2	Full-matrix least-squares on F^2
Data / restraints / parameters	3819 / 6 / 161	6671 / 6 / 307	11146 / 1 / 522
Goodness-of-fit on F^2	1.024	1.060	1.040
Final R indices [I>2sigma(I)]	R1 = 0.0356, wR2 = 0.0651	R1 = 0.0336, wR2 = 0.0577	R1 = 0.0442, wR2 = 0.0583
Final R indices (all data)	R1 = 0.0614, wR2 = 0.0707	R1 = 0.0646, wR2 = 0.0679	R1 = 0.0858, wR2 = 0.0674
Largest diff. peak and hole	1.167 and -2.052 e.$Å^{-3}$	0.988 and -1.166 e.$Å^{-3}$	0.849 and -1.091 e.$Å^{-3}$

Table S3 Crystal data and structure refinement for **DMA-Sb-I. I.O.I.H.M (4)**

Compound name	***DMA-Sb-I. I.O.I.H.M***
CCDC number	1910948
Empirical formula	C_{16} H_{38} I_9 N_4 O_4 Sb_2 (+ squeezed part)
Moiety formula representation	Sb_2I_9(DMA-H···DMA)$_2$ (+ squeezed part)
Formula weight	1736.10
Temperature	150(2) K
Wavelength	0.71073 Å
Crystal system	orthorhombic
Space group	'P n m a'
a	15.6538(5) Å
b	28.4872(10) Å
c	10.8182(4) Å
α, β, γ	90°, 90°, 90°
Volume	4824.2(3) Å^3
Z	4
Crystal size	210x90x16 mm
Density (calculated)	2.390 mg/m^3
Absorption coefficient	6.901 mm^{-1}
F(000)	3092
Theta range for data collection	2.288 to 28.329 °
Index ranges	-17<=h<=20 -37<=k<=37 -14 <=l<=14
Reflections collected	70909
Independent reflections	6124 [R(int) = 0.0927]

Completeness to theta = 25.242°	99.8 %
Refinement method	Full-matrix least-squares on F^2
Data / restraints / parameters	6124 / 0 / 174
Goodness-of-fit on F^2	1.106
Final R indices [I>2sigma(I)]	R1 = 0.0427, wR2 = 0.0774
Final R indices (all data)	R1 = 0.0811, wR2 = 0.0851
Largest diff. peak and hole	0.851 and -1.123 e.$Å^{-3}$

IX. Computational Methodology:

In order to validate the experimental outcome, we have rigorously performed electronic structure calculations based on Density Functional Theory (DFT) formalism for the newly synthesized crystal structure of **1**, **2** and **3** respectively. Throughout the first principles calculations, we have used Vienna Ab-initio Simulation Package (VASP) [1, 2]. The Perdew-Burke-Ernzerhof (PBE) type exchange correlation functional is used, which is in the framework of generalized gradient approximation (GGA) [3]. The lattice parameters and the space group of **1**, **2** and **3** respectively. crystal structure are consistent with the experimental values of the synthesized structure. In order to achieve a minimum energy configuration of the considered system, we have undertaken a full ionic relaxation until the corresponding Hellman-Feynman forces are getting smaller than 0.001 eV/A^o. We have used 5x5x5 Monkhorst-Pack k-points while performing the ionic relaxation of the system. After getting the optimized structure with minimum most energy, we determine the projected density of states (PDOS) to know the elemental contribution towards the total DOS of **1**, **2** and **3** and the optical absorption spectra. To calculate the optical absorption spectra, we consider double the number of occupied states in order to have adequate number of unoccupied states for the

allowed transitions between valance and conduction bands. The variation of the optical absorption cross section as a function of photon energy leads to the absorption spectra in this way, which is determined based on the frequency dependent dielectric function $\varepsilon(\omega) = \varepsilon_1(\omega) + i\varepsilon_2(\omega)$. The sum over the unoccupied bands using Fermi's Golden rule gives rise to the imaginary part $\varepsilon_2(\omega)$.

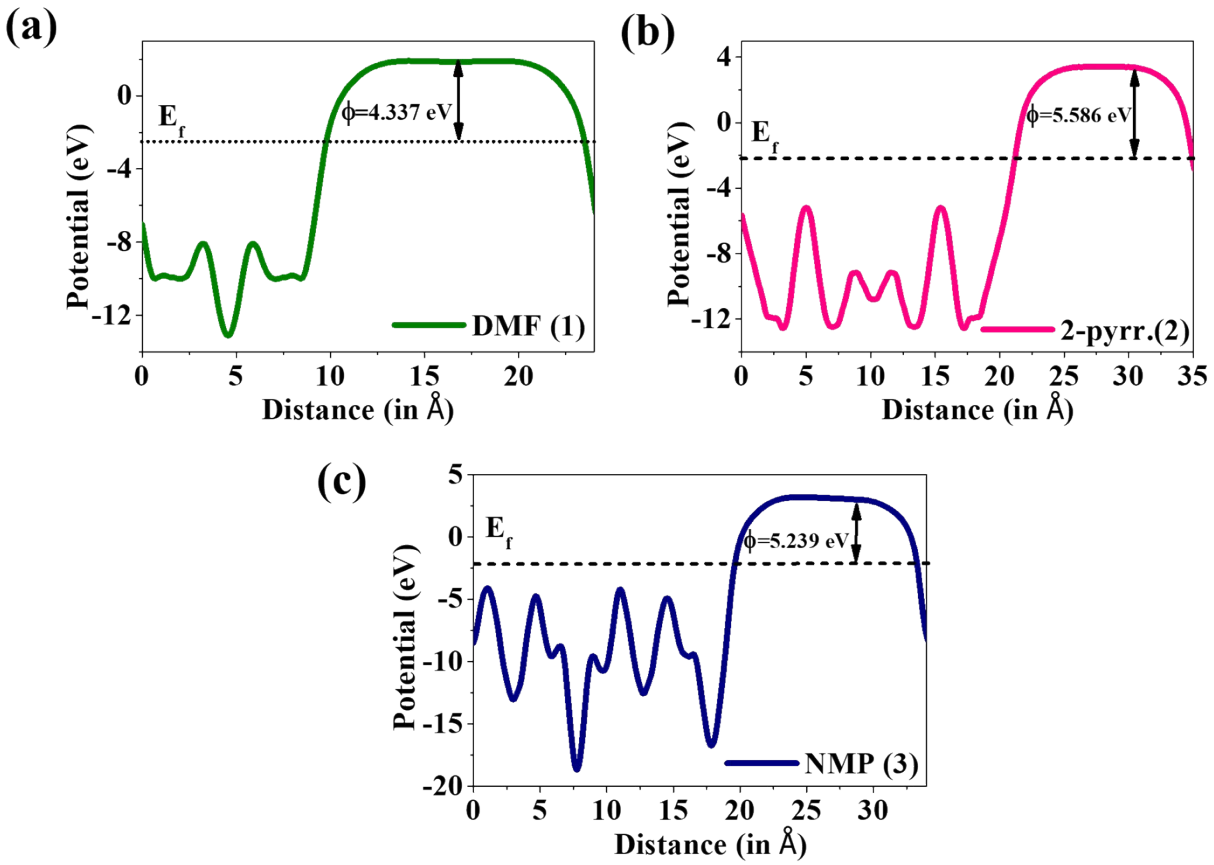

Figure S8 Work function evaluated by DFT calculation of **1**, **2** and **3** respectively.

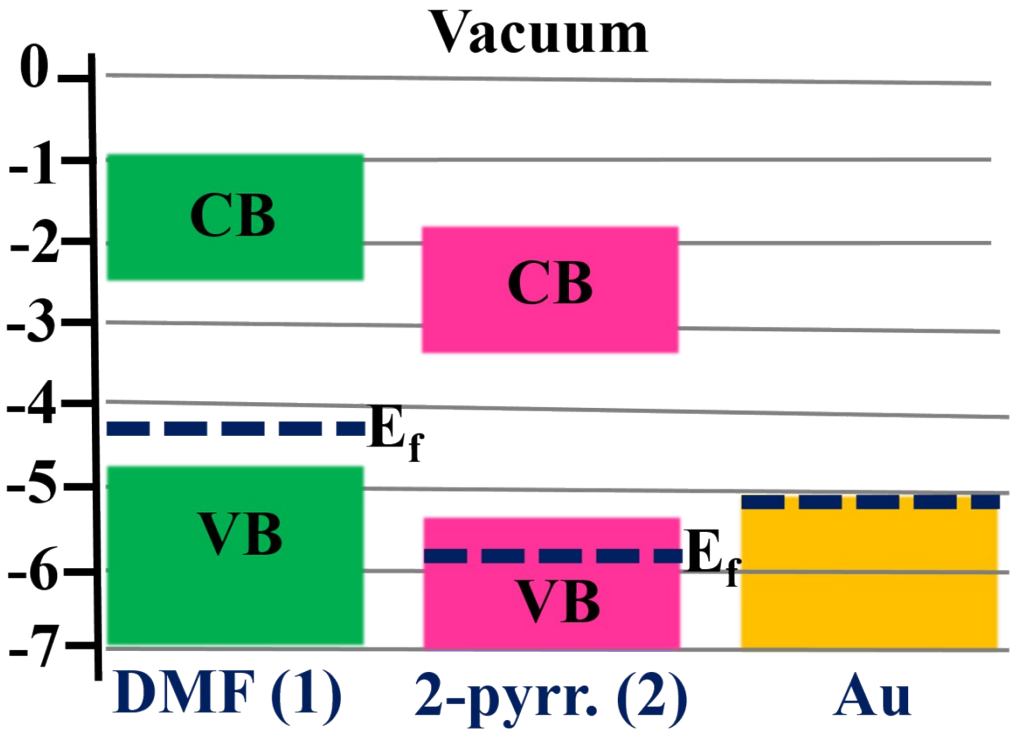

Figure S9 Energy band alignment of Au/**1** and Au/**2** based thin film heterostructure.

References

[1] Kresse, G., Furthmüller J., Efficient iterative schemes for ab initio total-energy calculations using a plane-wave basis set. Phys. Rev. B 1996, 54 (16), 11169-11186 DOI: 10.1103/PhysRevB.54.11169.

[2] Kresse, G.; Hafner, J. Ab initio molecular dynamics for liquid metals. Phys. Rev. B 1993, 47 (1), 558–561 DOI: 10.1103/PhysRevB.47.558.

[3] Perdew, J. P., Burke, K., Ernzerhof, M. Generalized, gradient approximation made simple. Phys. Rev. Lett. 1996, 77 (18), 3865–3868.

[4] George C. Anyfantis, Nikolaos-Minas Ganotopoulos, Aikaterini Savvidou, Catherine P. Raptopoulou,Vassilis Psycharis and George A. Mousdis, Synthesis and characterization of new organic–inorganic hybrid compounds based on Sb, with a perovskite like structure, *Polyhedron*, 2018, **151**, 299–305.